Original Article
J. Korean Wood Sci. Technol. 2023, 51(1): 1-13
https://doi.org/10.5658/WOOD.2023.51.1.1

Journal of the Korean Wood Science and Technology
pISSN: 1017-0715 eISSN: 2233-7180
http://www.woodj.org

Characteristics of Magnetic Sengon Wood Impregnated with Nano Fe_3O_4 and Furfuryl Alcohol

Gilang Dwi LAKSONO[1] · Istie Sekartining RAHAYU[1,†] · Lina KARLINASARI[1] · Wayan DARMAWAN[1] · Esti PRIHATINI[1]

ABSTRACT

Sengon (*Falcataria moluccana* Miq.) tree offers a wood of low quality and durability owing to its low density and thin cell walls. This study aimed to improve the properties of sengon wood by making the wood magnetic, producing new functions, and characterizing magnetic sengon wood. Each wood sample was treated using one of the following impregnation solutions: Untreated, 7.5% nano magnetite-furfuryl alcohol (Fe_3O_4-FA), 10% nano Fe_3O_4-FA, and 12.5% nano Fe_3O_4-FA. The impregnation process began with vacuum treatment at 0.5 bar for 2 h, followed by applying a pressure of 1 bar for 2 h. The samples were then tested for dimensional stability and density and characterized using scanning electron microscopy and energy-dispersive X-ray spectroscopy (SEM–EDX), Fourier transform infrared spectrometry (FTIR), X-ray diffraction (XRD) analysis, and vibrating sample magnetometry (VSM) analysis. The results showed that the Fe_3O_4-FA impregnation treatment considerable affected the dimensional stability, measured in terms of weight percent gain, anti-swelling efficiency, water uptake, and bulking effect, as well as the density of sengon wood. Changes in wood morphology were detected by the presence of Fe deposits in the cell walls and cell cavities of the wood using SEM–EDX analysis. XRD and FTIR analyses showed the appearance of magnetite peaks in the diffractogram and Fe-O functional groups. Based on the VSM analysis, treated sengon wood is classified as a superparamagnetic material with soft magnetic properties. Overall, 10% Fe_3O_4-FA treatment led to the highest increase in dimensional stability and density of sengon wood.

Keywords: dimensional stability, furfuryl alcohol, impregnation, magnetic wood, nano Fe_3O_4, sengon wood

1. INTRODUCTION

Indonesia cultivates many types of fast-growing wood to overcome the shortage of raw materials and meet the needs of its population. Sengon (*Falcataria moluccana* Miq.) is a fast-growing wood species widely planted in Indonesia. Sengon wood is a light wood having a specific gravity of 0.33, ranging between 0.24−0.49, and belongs to the strength class IV−V and durability class IV−V (Martawijaya *et al*., 2005). Typically, sengon wood is typically used as a raw material for making wood crates, particleboards, fiberboards, matches, and handicrafts. The productivity of fast-growing wood is high, but it has several problems, especially those related to physical properties and others (Priadi *et al*., 2019). Bowyer *et al*. (2007) stated that fast-growing wood has

Date Received August 23, 2022, Date Revised September 15, 2022, Date Accepted November 4, 2022
[1] Department of Forest Products, Faculty of Forestry and Environment, IPB University, Bogor 16680, Indonesia
[†] Corresponding author: Istie Sekartining RAHAYU (e-mail: Istiesr@apps.ipb.ac.id, https://orcid.org/0000-0003-4902-564X)

disadvantages such as low density and durability. Therefore, it is necessary to improve the properties, produce new functions, and enable the broader application of wood.

In this study, we used the impregnation method to improve wood quality. Impregnation using vacuum pressure tubes can improve or enhance the physical properties of wood (Hadi *et al*., 2018; Hartono *et al*., 2016; Oh and Park, 2015). Wood impregnation involves introducing chemicals into pores, lumens, and cell walls to precipitate and store chemicals without damaging the wood. Impregnation methods have been applied to fast-growing wood to improve wood quality using chemicals such as methyl methacrylate (Cahyono *et al*., 2020; Hadi *et al*., 2019), phenol-formaldehyde (Sumardi *et al*., 2020), melamine formaldehyde, furfuryl alcohol (FA); (Prihatini *et al*., 2020), nano TiO_2 (Rahayu *et al*., 2022b) and magnetite (Fe_3O_4) nanoparticles (Rahayu *et al*., 2022a).

One of the materials used in manufacturing includes nano iron oxides, such as Fe_3O_4, widely used as a non-ferrofluid material (Kumar *et al*., 2010). Magnetite nanoparticles (nano Fe_3O_4) have been extensively applied in the manufacture of magnetically charged wood because these are easily synthesized and have good biocompatibility (Zhang *et al*., 2021). Wood impregnated with a magnetic liquid becomes magnetic wood, which has novel magnetic properties (Merk *et al*., 2014). Magnetic wood can be used as a construction material to retain heat (Oka *et al*., 2012) and can also be used in energy harvesting, adsorption, and removal of contaminants such as heavy metals, dyes, and organic pollutants (Sezer *et al*., 2021). In addition, magnetic wood offers many attractive characteristics, such as being able to attract or be attracted to magnets, absorb electromagnetic waves, and increase dimensional stability (Ayrilmis and Kaymakci, 2013; Trey *et al*., 2014).

Magnetic wood is composed of a combination of wood and a magnetic powder or magnetic liquid. Wood can be magnetized using both *ex-situ* and *in-situ* processes. The current study used the *ex-situ* method to manufacture magnetic wood because this method does not utilize strong and weak base precursors (Dong *et al*., 2016; Rahayu *et al*., 2022a) directly as in the *in situ* method, which could cause the degradation of lignin (Schmiedl *et al*., 2012), and the materials needed are easy to obtain. The *ex-situ* method involves impregnation with a solution containing nano Fe_3O_4, readily available in the market (Gan *et al*., 2017; Kumar *et al*., 2021; Tang and Fu, 2020).

The use of nano Fe_3O_4 to manufacture magnetic wood has limitations because the compound is washed easily out of the wood. In addition, it is unstable, readily agglomerates, and oxidizes (Masoudi *et al*., 2012; Theerdhala *et al*., 2010). Magnetic particles dispersed in a liquid have a natural tendency to interact with each other and form aggregates because of the attraction between them (Vennapusa *et al*., 2008). The weakness can be reduced or prevented by mixing nano Fe_3O_4 and demineralized water with FA, which acts as a dispersant. The nano Fe_3O_4 forms a colloidal phase when mixed with FA, which allows nano Fe_3O_4 to be impregnated more easily into the wood. Mixing with FA is also a practical and environmentally friendly approach for manufacturing magnetic wood. In addition, Dong *et al*. (2016) reported that using FA protected the nanoparticles from leaching, thereby increasing the dimensional stability of wood and supporting a high percentage of weight gain. This study aimed to analyze and characterize the physical properties of magnetic sengon wood, including density and dimensional stability.

2. MATERIALS and METHODS

2.1. Materials

A 43-cm-diameter log of sengon wood was sourced from a tree with a branch-free height of 7–9 m harvested in Sukabumi, Indonesia. Other materials used in the

study included nano Fe_3O_4 (particle diameter 297 ± 10 nm; Anhui Elite Industrial, Hefei, China), FA (Sigma Aldrich, St. Louis, MO, USA), and demineralized water.

2.2. Methods

2.2.1. Preparation of samples and impregnation solutions

Test samples measuring 2 × 2 × 2 cm (BS-373:1957) were cut out of sengon wood log. The samples were tested for weight percent gain (WPG), anti-swelling efficiency (ASE), water uptake (WU), bulking effect (BE), and density (ρ). The impregnation solution included demineralized water (untreated), nano Fe_3O_4 and FA (1:1 mol). In this study, three concentrations of nano Fe_3O_4 (w/v%) were used, namely 7.5%, 10%, and 12.5%. After the nano Fe_3O_4, and FA were mixed based on the treatment concentration, the impregnation solution was stirred for 15 min, followed by a sonication (Cole Parmer) with an amplitude of 40% for 30 min.

2.2.2. Impregnation process

The impregnation process was initiated by oven-drying the test sample at a temperature of 103 ± 2℃. Subsequently, the dimensions were measured and weighed. The test samples were then placed in a container, followed by adding the impregnation solution into the container. The test sample and solution were then placed into the impregnation tube under a vacuum of −0.5 bar for 2 h, followed by subjection to a pressure of 1 bar for 2 h. When the impregnation process was over, the test samples were wrapped in aluminum foil and dried in an oven at 65℃ for 12 h. After drying the test samples for 12 h, we removed the aluminum foil covering the samples and placed the samples back into the oven for drying at a temperature of 103 ± 2℃ until the samples achieved a constant weight. The impregnated test samples were then immersed in demineralized water for 24 h and dried in an oven at 103 ± 2℃.

2.2.3. Physical properties of sengon magnetic wood

The physical properties of magnetic wood were tested according to Hill (2006) and Bowyer *et al*. (2007), including WPG, BE, density (ρ), ASE, and WU, using the following formulas:

$$WPG\ (\%) = [(W_1 - W_0) / W_0] \times 100$$
$$ASE\ (\%) = [(Su - St) / Su] \times 100$$
$$WU\ (\%) = [(W_2 - W_1) / W_1] \times 100$$
$$BE\ (\%) = (V_1 - V_0) / V_0 \times 100$$
$$\rho\ (g/cm^3) = (W_1 / V_1) \times 100$$

where,

W_0 = Sample oven-dried weight before impregnation treatment (g)

W_1 = Sample oven-dried weight after impregnation treatment (g)

W_2 = Sample weight after being immersed in water for 24 hours (g)

V_0 = Sample oven-dried volume before impregnation treatment (cm^3)

V_1 = Sample oven-dried volume after impregnation treatment (cm^3)

Su = Volume shrinkage of the untreated sample

St = Volume shrinkage of the treated sample

2.3. Characterization of magnetic sengon wood

2.3.1. Scanning electron microscopy–Energy-dispersive X-ray spectroscopy (SEM–EDX) analysis

The penetration and distribution of nano Fe_3O_4 in the wood cell walls were analyzed using SEM (JEOL JSM-6510LA series). The untreated and impregnated wood samples were cut to a size of 0.5 cm × 0.5 cm × 0.5 cm on a tangential plane, placed on conductor adhesive, coated with gold, and observed under SEM at a voltage

of 20 kV. Wood samples were also analyzed using EDX to determine the chemical content of the wood (Rahayu *et al*. 2022a).

2.3.2. Fourier transform infrared spectrometry (FTIR) analysis

Untreated and impregnated wood samples were milled into 200-mesh particles and embedded in potassium bromide pellets. Then, the finished pellets were analyzed using FTIR (Perkin-Elmer Spectrum One) and scanned in the wavenumber range of 4,000–400 cm^{-1} with a resolution of 4 cm^{-1} for 32 scans (Rahayu *et al*. 2022a).

2.3.3. X-ray diffraction (XRD) analysis

Wood samples were cut into 2-mm-thick pieces in a tangential direction. The degree of crystallinity of the wood sample (incision) was analyzed using an XRD (PANanalytical Empyrean) instrument with a 1D PIXcel detector. The parameters used in the device were Cu Kα radiation with a graphite monochromator, a voltage of 40 kV, a current of 30 mA, and a scan range of 2θ between 5° and 80° for the degree of crystallinity and between 5° and 90° for phase analysis. The scanning speed was set at 2°/min (Rahayu *et al*. 2022a).

2.3.4. Vibrating sample magnetometry (VSM) analysis

The magnetic loop hysteresis of the differentially treated wood specimens was determined using a Lake Shore 7410 VSM meter (Lake Shore Cryotronics, Westerville, OH, USA) at 300 K outside the magnetic field from −20 to 20 kOe in 100 Oe steps and a mean time of 100 ms. In addition, the saturation magnetization (M_s), coercivity (H_c), and remanence (M_r) were evaluated from the hysteresis curve. The magnetic properties of the samples were evaluated using VSM. The dimensions of the specimens for the magnetic test were 3 mm × 3 mm × 7 mm in the longitudinal direction (Rahayu *et al*. 2022a).

2.4. Statistical analyses

This study used a completely randomized design, and data were evaluated using an analysis of variance followed by Duncan's test at α = 1%. Statistical analyses were performed using IBM SPSS version 25.0.

3. RESULTS and DISCUSSION

3.1. Dimensional stability of sengon wood

The density, WPG, BE, WU, and ASE of untreated and treated samples are presented in Table 1. Compared with untreated wood, the density, WPG, BE, and ASE values of sengon wood treated with Fe_3O_4-FA increased, whereas the WU value decreased, revealing considerable differences from the values for untreated wood samples. The increased dimensional stability and density observed in this study agree with the results of Dong *et al*. (2016)

Table 1. Data on the dimensional stability of sengon wood

Treatment	WPG (%)	BE (%)	Density (g/cm^3)	WU (%)	ASE (%)
Untreated	0.00^a	3.28^a (± 0.37)	0.24^a (± 0.02)	153.63^a (± 26.73)	0.00^a
7.5% Fe_3O_4-FA	28.98^b (± 1.20)	4.23^b (± 1.00)	0.37^b (± 0.05)	53.01^b (± 11.12)	67.33^b (± 16.65)
10% Fe_3O_4-FA	34.69^c (± 3.24)	5.03^b (± 0.16)	0.39^b (± 0.02)	49.29^b (± 19.14)	61.52^b (± 22.62)
12.5% Fe_3O_4-FA	33.46^c (± 3.69)	4.50^b (± 0.48)	0.38^b (± 0.02)	39.05^b (± 13.31)	82.40^b (± 13.06)

$^{a-c}$ Values followed by different letters are significantly different (p-value < 0.01), based on Duncan's test.
WPG: weight percent gain, BE: bulking effect, WU: water uptake, ASE: anti-swelling efficiency, FA: furfuryl alcohol.

and Rahayu *et al*. (2022a), who reported the same trends in poplar and jabon wood.

The WPG value of treated samples increased with the concentration of Fe_3O_4-FA, with the 10% Fe_3O_4-FA treatment resulting in the highest WPG value. The WPG value of sengon wood treated with Fe_3O_4-FA was higher than that of the untreated wood. The result is in agreement with that of a previous study by Dirna *et al*. (2020), reporting higher WPG values of fast-growing wood when impregnated with monoethylene glycol and nano-silica, and that of Hartono *et al*. (2016), also observing the same trend in oil palm trunks when impregnated using phenol–formaldehyde. The WPG of the sample treated using 12.5% Fe_3O_4-FA is lower than that of sengon treated with 10% Fe_3O_4-FA because the size of Fe_3O_4 at a concentration of 12.5% is greater than that at a concentration of 10% (for details see discussion of the XRD analysis). Moreover, the Fe_3O_4 solution is denser and thicker at 12.5% concentration. Therefore, it is difficult for nano Fe_3O_4 to enter and penetrate sengon wood, which only covers the surface of the wood at 12.5% concentration. However, based on Duncan's test results, WPG values between 10% and 12.5% were not significantly different (p-value < 0.01).

The increase in the density of sengon wood in this study was followed by increased WPG value in agreement with the results of Hadi *et al*. (2022), who reported that the furfurylated sample had a higher density than the untreated sample and the increase in WPG value followed the increase in density. The higher the density of the treated wood, the greater the content that filled the wood cell walls and the thicker the wood cell walls (Bowyer *et al*., 2007). Wood density is a critical factor in determining the physical properties of wood (Lee and Lee, 2018; Zhang *et al*., 2018). The impregnation treatment with Fe_3O_4 and FA solutions resulted in the penetration of these solutions into the wood cell walls, resulting in the formation of bonds with the wood cell wall components, which caused the cell walls to swell and fill the microvoids in the cell walls (Hadiyane *et al*., 2018; Hill, 2006).

The ASE and BE values tended to increase with treatment. The increase in the ASE value with impregnation treatment was in agreement with Priadi *et al*. (2020). Adding Fe_3O_4 and FA to sengon wood makes the treated wood denser and has higher dimensional stability. Prihatini *et al*. (2020) showed that FA combined with melamine-formaldehyde increased the BE values. The higher the BE value, the more the polymer fills the cell wall, thereby increasing dimensional stability (Hill, 2006). The WU value showed a decreasing trend with treatment. This indicates that less water can enter the wood. The addition of FA can form a barrier on the lumen surface and reduce water absorption. However, the hydrophobic nature of FA also affects its water-repellent properties (Dong *et al*., 2014).

3.2. Magnetic sengon wood characteristics

3.2.1. Scanning electron microscopy–Energy-dispersive X-ray spectroscopy (SEM–EDX) analysis

The morphologies of the untreated and impregnated sengon wood were observed using SEM (Fig. 1). The condition of the wood that initially appeared empty [Fig. 1(a)]. After impregnation, the treated wood looked like nano Fe_3O_4-FA covering the cell walls, and deposits were also present in the intercellular spaces marked with color (yellow) in Fig. 1(b), (c), and (d). Yellow spots were observed, indicating the presence of nano Fe_3O_4 and FA on sengon wood treated with Fe_3O_4-FA 7.5%, 10%, and 12.5%. The presence of nano Fe_3O_4-FA that enters and covers the wood cell walls has a BE on sengon wood. This can prevent the entry of water into the cell walls of the wood, which is indicated by the decreased WU value.

Sengon wood impregnated with Fe_3O_4-FA caused an increase in the weight of sengon wood, as evidenced by

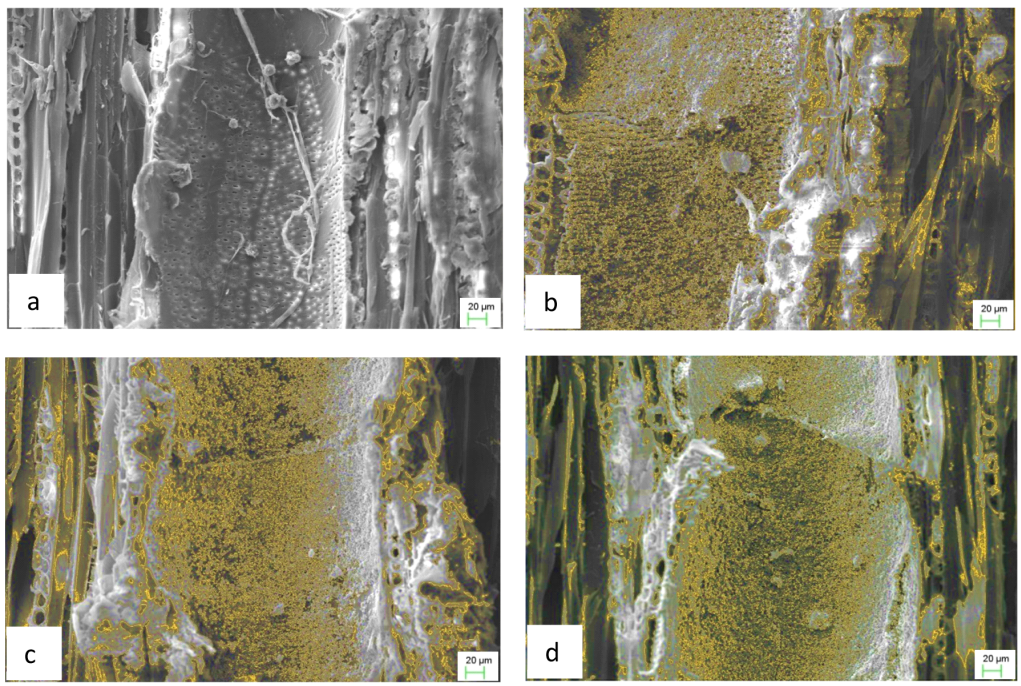

Fig. 1. Morphology of sengon wood that was (a) untreated, (b) 7.5% Fe_3O_4-FA, (c) 10% Fe_3O_4-FA, and (d) 12.5% Fe_3O_4-FA. FA: furfuryl alcohol.

an increase in the WPG value. Based on Dirna *et al*. (2020), the results of the SEM analysis revealed possible causes of an increase in the value of WPG, ASE, BE, and density and a decrease in the value of WU in treated sengon wood. According to Xue and Zhao (2008), nanoparticles can enter and penetrate wood, particularly through nanosized cavities. Additional information from the EDX analysis in (Table 2) indicates the presence of Fe that enters and covers the cell walls of impregnated sengon wood. The percentage of Fe increased with increasing concentration of Fe_3O_4-FA solution from 23.53% to 59.63%. The morphological image and the results of the SEM-EDX test showed that nano-magnetite managed to enter, cover, and deposit on the sengon wood cell walls and cavities of the cells.

Table 2. Fe composition of sengon wood samples

Treatment	Fe (wt. %)
Untreated	0
7.5% Fe_3O_4-FA	23.53
10% Fe_3O_4-FA	49.07
12.5% Fe_3O_4-FA	59.63

FA: furfuryl alcohol.

3.2.2. Fourier transform infrared spectrometry (FTIR) analysis

The FTIR results are shown in Fig. 2. The wave numbers 3,337 cm^{-1}, 3,341 cm^{-1}, and 3,336 cm^{-1} in each sample indicate the presence of O-H stretching functional groups. According to Xu *et al*. (2019), the O-H functional group is indicated by the wave number 3,200–3,600 cm^{-1} and ranges from 3,570 cm^{-1} to 3,200 cm^{-1} (Nandiyanto *et al*., 2019). The detected peak vibrations ranged from 2,895 cm^{-1} to 2,922 cm^{-1}, which was associated with the presence of asymmetric C-H functional

groups and symmetrical strain vibrations (Gan *et al*., 2017; Wang *et al*., 2011), and the peak was observed at the wave number 1,727 cm^{-1}, 1,730 cm^{-1}, and 1,731 cm^{-1}, which are characterized by the C = O stretch of unconjugated ketone and ester groups from hemicellulose, and the side chains of lignin were broken by magnetic treatment (Chang and Chang, 2006; Rahman *et al*., 2011).

In addition, the weakening of the C-O functional group was also detected in this study, based on the findings of Rahayu *et al*. (2021) and Wahyuningtyas *et al*. (2022), who reported a weakening of the peak of the C-O functional group caused by the furan ring from FA at a wave number of 1,030 cm^{-1}, and Xu *et al*. (2019), who reported a wave number of 1,032 cm^{-1}. Wave numbers of 560 cm^{-1}, 562 cm^{-1}, and 560 cm^{-1} were seen when the sengon wood was impregnated. This indicates the presence of Fe-O functional groups in the sengon wood at each concentration. This finding indicates that Fe_3O_4 particles were deposited on the wood substrate. The Fe-O functional group detected in this study agrees with the results reported by Lin and Ho (2014), who found the peak of the Fe-O group at wave number 436–580 cm^{-1}.

3.2.3. X-ray diffraction (XRD) analysis

Fig. 3 presents the results of the XRD analysis of sengon wood, which has peaks at 2θ values of 21.94° and 34.53° with crystal planes (012); (Rahayu *et al*., 2022a) and (040) showing cellulose (Cave, 1997; Dong *et al*., 2016). After the sengon wood was treated, cellulose was still detected, but the degree of crystallinity could not be determined because of the strong magnetite diffraction background (Rahayu *et al*., 2022a). After sengon wood was treated, the two peaks were weakened, and the latter one may be covered by other peaks, indicating that part of the crystal structure in the wood was damaged by magnetic treatment (Dong *et al*., 2016). Several quasi-crystalline regions in hemicellulose and cellulose contribute to wood crystallinity (Bhuiyan *et al*., 2000).

Wood impregnated with Fe_3O_4-FA produced new peaks, indicating the formation of magnetite compounds in the wood. These peaks occur at the values of 2θ 35.35°, 35.20°, and 35.46° with the crystal plane (311); values of 2θ 43.00°, 42.82°, and 43.10° with crystal planes (400); values of 2θ 43.00°, 42.82°, and 43.10° with crystal planes (400); values of 2θ 56.94°, 56.81°,

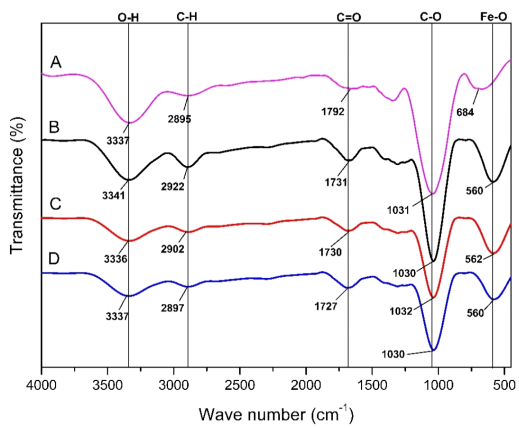

Fig. 2. FTIR analysis of sengon wood that (a) untreated, (b) 7.5% Fe_3O_4-FA, (c) 10% Fe_3O_4-FA, and (d) 12.5% Fe_3O_4-FA. FTIR: Fourier transform infrared spectrometry, FA: furfuryl alcohol.

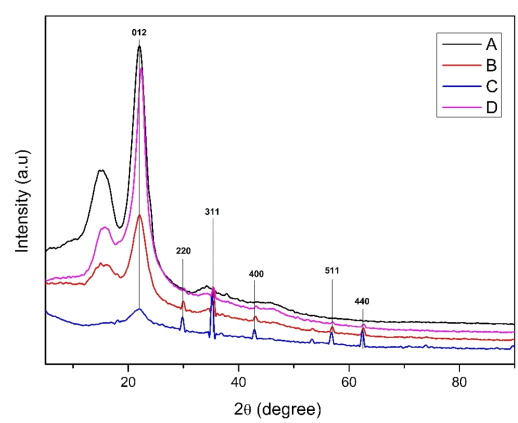

Fig. 3. XRD analysis of sengon wood that was (a) untreated, (b) 7.5% Fe_3O_4-FA, (c) 10% Fe_3O_4-FA, and (d) 12.5% Fe_3O_4-FA. XRD: X-ray diffraction, FA: furfuryl alcohol.

and 56.92° with crystal planes (511); and values of 2θ 62.57°, 62.36°, and 62.67° with crystal planes (440); (Wu *et al*., 2011). Fe_3O_4 peaks occur at approximately 30.1°, 35.4°, 43.1°, 53.4°, 56.9°, and 62.5°, based on the Joint Committee on Powder Diffraction Standard (JCPDS) magnetite card (No. 19-0629); (Yu and Kwak, 2010). The result is in agreement with the findings of Rahayu *et al*. (2022a) and Dong *et al*. (2016), who showed the presence of magnetite compounds in the presence of these peaks. After the treatment, all diffraction peaks belonging to Fe_3O_4 and wood were present in the magnetic wood, indicating that the Fe_3O_4 magnetic particles were successfully deposited on the wood substrate (Gan *et al*., 2017).

The size of Fe_3O_4 concentrations of 10% and 12.5% in sengon wood was determined based on the XRD diffractogram using the Scherrer equation (Lin and Ho, 2014).

$$D = \frac{K\lambda}{\beta \cos\theta}$$

where λ is the X-ray wavelength (0.15418 nm), K is the Scherrer constant (0.89), β is the peak full width at half maximum (FWHM), and θ is the Bragg diffraction angle (Dong *et al*., 2016). Based on the calculation results, the size of the 10% Fe_3O_4 concentration was 31.72 nm and the 12% concentration was 41.25 nm. The resulting size was in the nanoscale. According to Khan *et al*. (2019), if the size is in the range of 1−100 nm, it is classified as nanosized. The most important physical properties of materials that affect solubility are particle size, crystals smaller than 1 m, and high surface area can increase solubility (Cornell and Schwertmann, 2006).

3.2.4. Vibrating sample magnetometry (VSM) analysis

VSM testing of treated sengon wood produces a curve called a magnetization curve or hysteresis loop. The magnetic hysteresis curves of the sengon wood samples treated with various Fe_3O_4-FA concentrations are shown in Fig. 4. In addition, when an object is exposed to an external magnetic field or the magnetic field is removed, the hysteresis curve has a reverse current that is almost symmetrical and is also observed in the area of the hysteresis curve (Tebriani, 2019). The area of the hysteresis curve indicates the energy required for magnetization. The hysteresis curve generated by VSM is characterized by saturation magnetization (M_s), remanence (M_r), and coercivity (H_c).

The values of M_s-, M_r-, and H_c-treated sengon wood are shown in detail in Table 3. The M_s values for sengon wood with Fe_3O_4-FA concentrations of 7.5%, 10%, and 12.5% were 0.685, 1.710, and 1.248 emu/g, respectively. Magnetic sengon wood made with a 10% concentration had a higher M_s value, while the concentration of 7.5% was the lowest. According to Gao *et al*. (2012), the M_s value is related to the WPG value; the higher the WPG value, the higher the M_s value. The different saturation magnetization values are caused by several factors, namely, the grain size of the nanoparticles and the degree of crystallinity (Riyanto, 2012; Setiadi *et al*., 2013). The correlation between the WPG and M_s is

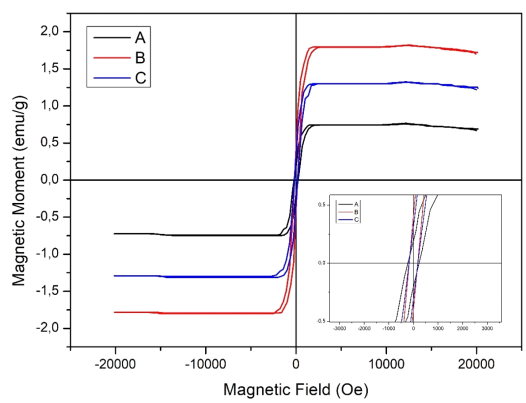

Fig. 4. VSM analysis of sengon wood that was (a) 7.5% Fe_3O_4-FA, (b) 10% Fe_3O_4 FA, and (c) 12.5% Fe_3O_4-FA. VSM: vibrating sample magnetometry, FA: furfuryl alcohol.

Table 3. The saturation magnetization (M_s), coercivity (H_c), and remanence (M_r) of the treated sengon wood

Treatment	M_s (emu/g)	M_r (emu/g)	H_c (O_e)
7.5% Fe_3O_4-FA	0.685	0.192	2.28×10^{-7}
10% Fe_3O_4-FA	1.710	0.409	1.87×10^{-6}
12.5% Fe_3O_4-FA	1.248	0.310	1.08×10^{-7}

FA: furfuryl alcohol.

shown in Fig. 5. The WPG value shows a linear correlation with the M_s value, indicating that the higher the WPG value, the greater the M_s value obtained. This is evident from the coefficient of determination, which is close to 1 (Chicco *et al*., 2021) and 0.9968. Similar results were reported by Dong *et al*. (2016) and Rahayu *et al*. (2022a). The M_s value in this study was lower than that of bulk nano-magnetite (Gan *et al*., 2017).

The M_r values for sengon wood impregnated using Fe_3O_4–FA concentrations of 7.5%, 10%, and 12.5% were 0.192, 0.409, and 0.310 emu/g, respectively. The M_r values in this study were greater than those in Rahayu *et al*. (2022a) and Moya *et al*. (2022), which stated that the M_r values of magnetic wood impregnated using the *in-situ* method were 0.01 emu/g and 0.01 to 0.25 emu/g,

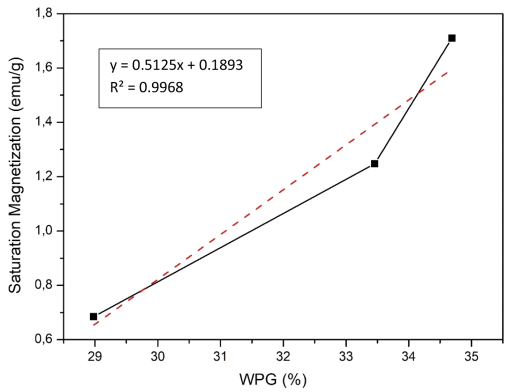

Fig. 5. Correlation between weight percent gain (WPG) and saturation magnetization (M_s) of treated sengon wood.

respectively. The M_r value increased with increasing concentrations of the Fe_3O_4-FA solution, although, at a concentration of 12.5%, the M_r value decreased. The result agrees with the observation of Wicaksono *et al*. (2013) that the greater the Fe_3O_4 concentrations in the formation, the greater the residual magnetism.

The H_c values for sengon wood with Fe_3O_4–FA concentrations of 7.5%, 10%, and 12.5% were 2.28×10^{-8} Oe, 1.87×10^{-6} Oe, and 1.08×10^{-7} Oe, respectively. The H_c value of sengon wood treated with Fe_3O_4–FA was classified as the low coercivity field value. This can be said to be low because the H_c value is almost zero or small and the area of the hysteresis curve tends to be narrow and slender. This indicates that the magnetic sengon wood may have superparamagnetic properties, as can be seen from the H_c value, which is close to zero (Hui *et al*., 2008; Rahayu *et al*., 2022a; Xu *et al*., 2005). In addition, magnetic sengon wood was included in the soft magnetic-type category (Karbeka *et al*., 2020; Marta *et al*., 2020; Widanarto *et al*., 2015). Soft Magnetic Properties are easily influenced by the external magnetic field, which is easily magnetized, and the magnetic intensity easily returns to a value of 0 when the external magnetic field is removed (Wicaksono *et al*., 2018).

4. CONCLUSIONS

Impregnation treatment of sengon wood with nano Fe_3O_4 and FA concentration of 10% in several parameters, such as WPG, BE, and density, is optimal for the time being. The parameters of physical properties have an increasing trend (WPG, BE, density, and ASE) and a decreasing trend for WU. SEM results showed changes in the morphology of sengon wood, with the presence of Fe (yellow color), which covers and deposits the cell walls in the wood. The results of FTIR analysis showed the presence of Fe-O functional groups in the treated wood. The treated wood exhibited new peaks, indicating the formation of magnetite compounds in the wood (XRD

analysis). The sengon wood treated with Fe_3O_4–FA was classified as soft magnetic with superparamagnetic properties.

CONFLICT of INTEREST

No potential conflict of interest relevant to this article was reported.

ACKNOWLEDGMENT

The authors are grateful for the support of the ministry of education, culture and research and technology of Indonesia (grant no 89/E1/KPT/2021 and grant no. 077/E4.1/AK.04.PT/2021).

REFERENCES

Ayrilmis, N., Kaymakci, A. 2013. Fast growing biomass as reinforcing filler in thermoplastic composites: *Paulownia elongata* wood. Industrial Crops and Products 43: 457-464.

Bhuiyan, M.T.R., Hirai, N., Sobue, N. 2000. Changes of crystallinity in wood cellulose by heat treatment under dried and moist conditions. Journal of Wood Science 46(6): 431-436.

Bowyer, J.L., Bowyer, J.L., Shmulsky, R., Haygreen, J.G. 2007. Forest Products and Wood Science: An Introduction. 5th ed. Iowa State Press, Ames, IA, USA.

British Standards Institution. 1957. Method of Testing Small Clear Specimens of Timber (BS 373: 1957). British Standards Institution, London, UK.

Cahyono, T.D., Darmawan, W., Priadi, T., Iswanto, A.H. 2020. Flexural properties of heat-treatment samama (*Anthocephalus macrophyllus*) wood impregnated by boron and methyl metacrylate. Journal of the Korean Wood Science and Technology 48(1): 76-85.

Cave, I.D. 1997. Theory of X-ray measurement of microfibril angle in wood. Wood Science and Technology 31(3): 143-152.

Chang, H.T., Chang, S.T. 2006. Modification of wood with isopropyl glycidyl ether and its effects on decay resistance and light stability. Bioresource Technology 97(11): 1265-1271.

Chicco, D., Warrens, M.J., Jurman, G. 2021. The coefficient of determination R-squared is more informative than SMAPE, MAE, MAPE, MSE and RMSE in regression analysis evaluation. PeerJ Computer Science 7: e623.

Cornell R.M., Schwertmann U. 2006. The Iron Oxides: Structure, Properties, Reactions, Occurrences and Ues. John Wiley & Sons, New York, NY, USA.

Dirna, F.C., Rahayu, I., Zaini, L.H., Darmawan, W., Prihatini, E. 2020. Improvement of fast-growing wood species characteristics by MEG and nano SiO_2 impregnation. Journal of the Korean Wood Science and Technology 48(1): 41-49.

Dong, Y., Yan, Y., Zhang, S., Li, J. 2014. Wood/polymer nanocomposites prepared by impregnation with furfuryl alcohol and nano SiO_2. BioResources 9(4): 6028-6040.

Dong, Y., Yan, Y., Zhang, Y., Zhang, S., Li, J. 2016. Combined treatment for conversion of fast-growing poplar wood to magnetic wood with high dimensional stability. Wood Science and Technology 50(3): 503-517.

Gan, W., Gao, L., Xiao, S., Gao, R., Zhang, W., Li, J., Zhan, X. 2017. Magnetic wood as an effective induction heating material: Magnetocaloric effect and thermal insulation. Advanced Materials Interfaces 4(22): 1700777.

Gao, H.L., Wu, G.Y., Guan, H.T., Zhang, G.L. 2012. *In situ* preparation and magnetic properties of Fe_3O_4/wood composite. Materials Technology 27(1): 101-103.

Hadi, Y.S., Herliyana, E.N., Pari, G., Pari, R., Abdillah, I.B. 2022. Furfurylation effects on discoloration and

physical-mechanical properties of wood from tropical plantation forests. Journal of the Korean Wood Science and Technology 50(1): 46-58.

Hadi, Y.S., Massijaya, M.Y., Zaini, L.H., Abdillah, I.B., Arsyad, W.O.M. 2018. Resistance of methyl methacrylate-impregnated wood to subterranean termite attack. Journal of the Korean Wood Science and Technology 46(6): 748-755.

Hadi, Y.S., Massijaya, M.Y., Zaini, L.H., Pari, R. 2019. Physical and mechanical properties of methyl methacrylate-impregnated wood from three fast-growing tropical tree species. Journal of the Korean Wood Science and Technology 47(3): 324-335.

Hadiyane, A., Dungani, R., Dewi, S.P., Rumidatul, A. 2018. Effect of chemical modification of jabon wood (*Anthocephalus cadamba* Miq.) on morphological structure and dimensional stability. Journal of Biological Sciences 18(4): 201-207.

Hartono, R., Hidayat, W., Wahyudi, I., Febrianto, F., Dwianto, W., Jang, J.H., Kim, N.H. 2016. Effect of phenol formaldehyde impregnation on the physical and mechanical properties of soft-inner part of oil palm trunk. Journal of the Korean Wood Science and Technology 44(6): 842-851.

Hill, C.A.S. 2006. Wood Modification: Chemical, Thermal and Other Processes. John Wiley & Sons, Chichester, UK.

Hui, C., Shen, C., Yang, T., Bao, L., Tian, J., Ding, H., Li, C., Gao, H.J. 2008. Large-scale Fe_3O_4 nanoparticles soluble in water synthesized by a facile method. The Journal of Physical Chemistry C 112(30): 11336-11339.

Karbeka, M., Koly, F.V.L., Tellu, N.M. 2020. Characterization of the magnetic properties of iron sand Puntaru Beach, Alor – NTT Regency. Lantanida Journal 8(2): 96-188.

Khan, I., Saeed, K., Khan, I. 2019. Nanoparticles: Properties, applications and toxicities. Arabian Journal of Chemistry 12(7): 908-931.

Kumar, R., Stephen Inbaraj, B., Chen, B.H. 2010. Surface modification of superparamagnetic iron nanoparticles with calcium salt of poly (γ-glutamic acid) as coating material. Materials Research Bulletin 45(11): 1603-1607.

Kumar, S., Singh, R., Singh, T.P., Batish, A. 2021. Investigations for magnetic properties of PLA-PVC-Fe_3O_4-wood dust blend for self-assembly applications. Journal of Thermoplastic Composite Materials 34(7): 929-951.

Lee, J.M., Lee, W.H. 2018. Dimensional stabilization through heat treatment of thermally compressed wood of Korean pine. Journal of the Korean Wood Science and Technology 46(5): 471-485.

Lin, C.C., Ho, J.M. 2014. Structural analysis and catalytic activity of Fe_3O_4 nanoparticles prepared by a facile co-precipitation method in a rotating packed bed. Ceramics International 40(7): 10275-10282.

Marta, R., Darvina, Y., Ramli., Desnita. 2020. Effect of $MnFe_3O_4$ composition on magnetic properties of $MnFe_3O_4$/PVDF nanocomposite prepared by spin coating method. Pillar of Physics 13: 42-50.

Martawijaya, A., Kartasujana, I., Kadir, K., Prawira, S.A. 2005. Indonesian Wood Atlas. Part I (In Indonesian). Ministry of Forestry, Bogor, Indonesia.

Masoudi, A., Hosseini, H.R.M., Shokrgozar, M.A., Ahmadi, R., Oghabian, M.A. 2012. The effect of poly (ethylene glycol) coating on colloidal stability of superparamagnetic iron oxide nanoparticles as potential MRI contrast agent. International Journal of Pharmaceutics 433(1-2): 129-141.

Merk, V., Chanana, M., Gierlinger, N., Hirt, A.M., Burgert, I. 2014. Hybrid wood materials with magnetic anisotropy dictated by the hierarchical cell structure. ACS Applied Materials & Interfaces 6(12): 9760-9767.

Nandiyanto, A.B.D., Oktiani, R., Ragadhita, R. 2019. How to read and interpret FTIR spectroscope of organic material. Indonesian Journal of Science &

Technology 4(1): 97-118.

Oh, S.W., Park, H.J. 2015. Vacuum pressure treatment of water-soluble melamine resin impregnation for improvement of mechanical property, abrasion resistance and incombustibility on softwood. Journal of the Korean Wood Science and Technology 43(6): 792-797.

Oka, H., Terui, M., Osada, H., Sekino, N., Namizaki, Y., Oka, H., Dawson, F.P. 2012. Electromagnetic wave absorption characteristics adjustment method of recycled powder-type magnetic wood for use as a building material. IEEE Transactions on Magnetics 48(11): 3498-3500.

Priadi, T., Orfian, G., Cahyono, T.D., Iswanto, A.H. 2020. Dimensional stability, color change, and durability of boron-MMA treated red jabon (*Antochephalus macrophyllus*) wood. Journal of the Korean Wood Science and Technology 48(3): 315-325.

Priadi, T., Sholihah, M., Karlinasari, L. 2019. Water absorption and dimensional stability of heat-treated fast-growing hardwoods. Journal of the Korean Wood Science and Technology 47(5): 567-578.

Prihatini, E., Maddu, A., Rahayu, I.S., Kurniati, M., Darmawan, W. 2020. Improvement of physical properties of jabon (*Anthocephalus cadamba*) through the impregnation of nano-SiO_2 and melamin formaldehyde furfuril alcohol copolymer. IOP Conference Series: Materials Science and Engineering 935(1): 012061.

Rahayu, I., Darmawan, W., Nawawi, D.S., Prihatini, E., Ismail, R., Laksono, G.D. 2022b. Physical properties of fast-growing wood-polymer nano composite synthesized through TiO_2 nanoparticle impregnation. Polymers 14(20): 4463.

Rahayu, I., Prihatini, E., Ismail, R., Darmawan, W., Karlinasari, L., Laksono, G.D. 2022a. Fast-growing magnetic wood synthesis by an *in-situ* method. Polymers 14(11): 2137.

Rahayu, I.S., Wahyuningtyas, I., Zaini, L.H., Darmawan, W., Maddu, A., Prihatini, E. 2021. Physical properties of impregnated ganitri wood by furfuryl alcohol and nano-SiO_2. In: Mataram, Indonesia, Proceedings of the 13th International Symposium of Indonesian Wood Research Society, p. 012012.

Rahman, M.R., Hamdan, S., Ahmed, A.S, Islam, M.S., Talib, Z.A., Abdullah, W.F.W., Che Mat, M.S. 2011. Thermogravimetric analysis and dynamic Young's modulus measurement of *N*,*N*-dimethylacetamide-impregnated wood polymer composites. Journal of Vinyl & Additive Technology 17(3): 177-183.

Riyanto, A. 2012. Synthesis of Fe_3O_4 nanoparticles and their potential as active materials on surface sensing biosensors based on SPR. M.S. Thesis, Postgraduate Program, Gadjah Mada University, Indonesia.

Schmiedl, D., Endisch, S., Pindel, E., Rückert, D., Reinhardt, S., Unkelbach, G., Schweppe, R. 2012. Base catalyzed degradation of lignin for the generation of oxy-aromatic compounds: Possibilities and challenges. Erdöl Erdgas Kohle 128(10): 357-363.

Setiadi, E.A., Shabrina, N., Retno, H., Utami, B., Fahmi, N.F. 2013. Synthesis of cobalt ferrite ($CoFe_2O_4$) nanoparticles by coprecipitation method and characterization of their magnetic properties. Indonesian Journal of Applied Physics 3(1): 55-62.

Sezer, N., Arı, İ., Biçer, Y., Koç, M. 2021. Superparamagnetic nanoarchitectures: Multimodal functionalities and applications. Journal of Magnetism and Magnetic Materials 538: 168300.

Sumardi, I., Darwis, A., Saad, S., Rofii, M.N. 2020. Quality enhancement of falcataria-wood through impregnation. Journal of the Korean Wood Science and Technology 48(5): 722-731.

Tang, T., Fu, Y. 2020. Formation of chitosan/sodium phytate/nano-Fe_3O_4 magnetic coatings on wood surfaces via layer-by-layer self-assembly. Coatings 10(1): 51.

Tebriani, S. 2019. Analysis of the vibrating sample magnetometer (VSM) on the results of the electrodepo-

sition of a thin layer of magnetite using a continuous direct current. Natural Science Journal 5(1): 722-730.

Theerdhala, S., Bahadur, D., Vitta, S., Perkas, N., Zhong, Z., Gedanken, A. 2010. Sonochemical stabilization of ultrafine colloidal biocompatible magnetite nanoparticles using amino acid, L-arginine, for possible bio applications. Ultrasonics Sonochemistry 17(4): 730-737.

Trey, S., Olsson, R.T., Ström, V., Berglund, L., Johansson, M. 2014. Controlled deposition of magnetic particles within the 3-D template of wood: Making use of the natural hierarchical structure of wood. RSC Advances 4(67): 35678-35685.

Vennapusa, R.R., Hunegnaw, S.M., Cabrera, R.B., Fernández-Lahore, M. 2008. Assessing adsorbent–biomass interactions during expanded bed adsorption onto ion exchangers utilizing surface energetics. Journal of Chromatography A 1181(1-2): 9-20.

Wahyuningtyas, I, Rahayu, I., Maddu, A., Prihatini, E. 2022. Magnetic properties of wood treated with nano-magnetite and furfuryl alcohol impregnation. Bioresources 17(4): 6496-6510.

Wang, C., Piao, C., Lucas, C. 2011. Synthesis and characterization of superhydrophobic wood surfaces. Journal of Applied Polymer Science 119(3): 1667-1672.

Wicaksono, A., Rohman, L., Supriyanto, E. 2018. $BaFe_{12}O_{19}$ ferromagnetic resonance study using micromagnetic simulation. Scientific Periodic 6(1): 46-48.

Wicaksono, R., Yulianto, A., Sulhadi. 2013. Manufacture and characterization of barium ferrite-based composite magnets with natural rubber binders. Unnes Physics Journal 2(2): 32-36.

Widanarto, W., Fauzi, F. N., Cahyanto, W. T., Effendi, M. 2015. Improved magnetic properties of hematite through barium substitution and sintering temperature control. Physics Periodic 18(4): 125-130.

Wu, S., Sun, A., Zhai, F., Wang, J., Xu, W., Zhang, Q., Volinsky, A.A. 2011. Fe_3O_4 magnetic nanoparticles synthesis from tailings by ultrasonic chemical co-precipitation. Materials Letters 65(12): 1882-1884.

Xu, L., Xiong, Y., Dang, B., Ye, Z., Jin, C., Sun, Q., Yu, X. 2019. *In-situ* anchoring of Fe_3O_4/ZIF-67 dodecahedrons in highly compressible wood aerogel with excellent microwave absorption properties. Materials & Design 182: 108006.

Xu, Z.Z., Wang, C.C., Yang, W.L., Fu, S.K. 2005. Synthesis of superparamagnetic Fe_3O_4/SiO_2 composite particles via sol-gel process based on inverse miniemulsion. Journal of Materials Science 40(17): 4667-4669.

Xue, F., Zhao, G. 2008. Optimum preparation technology for Chinese fir wood/Ca-montmorillonite (Ca-MMT) composite board. Forestry Studies in China 10(3): 199-204.

Yu, B.Y., Kwak, S.Y. 2010. Assembly of magnetite nanocrystals into spherical mesoporous aggregates with a 3-D wormhole-like pore structure. Journal of Materials Chemistry 20(38): 8320-8328.

Zhang, M., Yao, A., Lin, J., Shi, P., Sun, G., Jin, C. 2021. Photothermally active borosilicate-based composite bone cement for near-infrared light controlled mineralisation. Materials Technology 27(10): 1243-1250.

Zhang, Y.H., Huang, Y.X., Ma, H.X., Yu, W.J., Qi, Y. 2018. Effect of different pressing processes and density on dimensional stability and mechanical properties of bamboo fiber-based composites. Journal of the Korean Wood Science and Technology 46(4): 355-361.